JOURNAL OF SOLID STATE CHEMISTRY 71, 47–60 (1987)

The Structures of Intergrowth Tungsten Bronzes of Ba, Sn, Pb, and Sb

M. M. DOBSON,* J. L. HUTCHISON,† R. J. D. TILLEY,* AND K. A. WATTS*

*Institute of Materials, University College, Newport Road, Cardiff CF2 1TA, and †Department of Metallurgy and Science of Materials, University of Oxford, Parks Road, Oxford, Great Britain

Received November 1, 1985; in revised form October 23, 1986

The structures of intergrowth tungsten bronzes (*ITB*) of compositions $Ba_{0.04}WO_3$, $Sn_{0.04}WO_3$, $Pb_{0.04}WO_3$, $Sn_{0.18}WO_3$, and $Sb_{0.25}WO_3$ have been deduced from high-resolution electron microscope images. Both the $Pb_{0.04}$, $Sn_{0.04}$, and $Ba_{0.04}$ *ITB* phases consist of single rows of hexagonal tunnels occupied by Pb, Sn, or Ba atoms intergrown in a WO_3-like matrix. The $Sb_{0.25}$ *ITB* phase is composed of similar rows of Sb-containing single hexagonal tunnels, the centers of which are separated by a WO_3-like matrix only two octahedra in thickness. The structure of the $Sn_{0.18}$ *ITB* phase consists of double rows of hexagonal tunnels containing Sn atoms joined by a single strip of WO_3-like octahedra. The structures are compared with the structures of other known *ITB* phases and the nonstoichiometric behavior of these phases is discussed.

Introduction

Intergrowth tungsten bronze (*ITB*) phases have a general formula M_xWO_3 and are a group of nonstoichiometric compounds which form in some *M*–W–O systems. The first phases to be labelled as *ITB* phases were described by Hussain and Kihlborg (*1, 2*). Electron microscope and X-ray crystallographic studies by these authors on materials in which *M* was either K, Cs, Rb, or Tl revealed that their structures consisted of double rows of hexagonal tunnels intergrown between slabs of WO_3-like material, as shown in Fig. 1a. The phases therefore represented intergrowths between WO_3 and the hexagonal tungsten bronze (*HTB*) structure type, hence the name proposed. The alkali metal atoms were located in the hexagonal tunnels. Later, single-row hexagonal tunnel structures were found in some Cs *ITB* phases (*3*), giving rise to the structure type shown in Fig. 1b. Since it therefore appears that both the width of the strips of hexagonal tunnels and the WO_3-like slabs in these compounds can vary, a series of closely related structures can arise. The variation in the stoichiometry of these phases can be thought of as accommodated by fluctuations in the degree of filling of the hexagonal tunnels present by the interpolated alkali metal atoms as well as by the variation in the number of tunnels present in the crystals.

Since these studies were conducted, a number of related phases, listed in Table I, have been found in the Bi–W–O (*4*), Sb–W–O (*5, 6*), and Sn–W–O (*7–9*) systems. In all of these compounds, strips of

0022-4596/87 $3.00

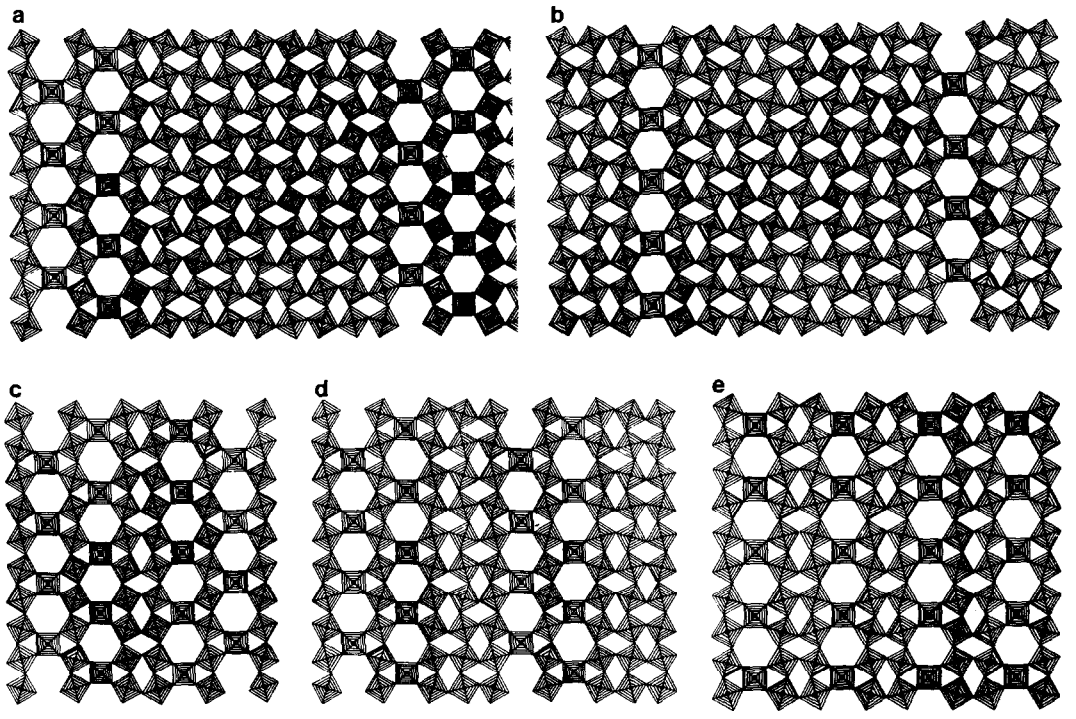

FIG. 1. The known *ITB* structures; (a) the double-tunnel structure of the alkali metal *ITB* phases; (b) the single-tunnel structure observed in some Cs and Bi *ITB* phases; (c) the structure of the 5-type Sn orthorhombic bronze; (d) the structure of the 6-type Sn orthorhombic bronze; (e) the proposed structure of the Sb *ITB*. In all of the drawings, only the WO_3 skeleton of the structure has been shown. In the real compounds the hexagonal tunnels are filled with the metal atoms referred to. In the case of the structures shown in (a) and (b), only one member of a series is illustrated. In these series, one member differs from another in the separation of the rows of hexagonal tunnels.

hexagonal tunnels are intergrown with strips of WO_3 type as illustrated in Figs. 1b–e. The compositions of these phases approach WO_3 as the amount of the WO_3-like slabs increases and that of the *HTB* structures as the number of hexagonal tunnels increases. When the amount of WO_3-like material decreases significantly a number of alternative ways of arranging the hexagonal tunnels have been found, as shown in Fig. 1.

Within recent years, a number of new bronze phases have been characterized in the Sn–W–O (*7–9*), Pb–W–O (*12*), and Ba–W–O (*13*) systems which have compositions of about $M_{0.04}WO_3$ and which have been shown to consist of slabs of WO_3-like structure linked by fault planes. Although it is likely that the structure of these phases is of the *ITB* type, this has not been confirmed experimentally. It was the primary purpose of this study to clarify these structures to verify that they indeed did belong to the same structural family as the *ITB* phases. In addition, the structures of Sn_xWO_3 and Sb_xWO_3 phases with compositions in the range $x = 0.15$–0.20 were in need of further study. This formed the second part of the work described here.

All phases were confirmed to be of the *ITB* type. The new phases are compared with known *ITB* structures and reasons for the formation of this structure type are discussed.

TABLE I

THE STRUCTURES OF INTERGROWTH AND RELATED TUNGSTEN BRONZE PHASES, M_xWO_3

Element M	Ionic size[a] (nm)	Composition range x	Structure
Cs	0.170	$0.06 < x < 0.10$	ITB; double and single tunnels
		$0.19 < x < 0.33$	HTB
Tl	0.150	$? < x < 0.10$	ITB; double tunnels
		$0.13 < x < 0.33$	HTB
Rb	0.149	$0.06 < x < 0.10$	ITB; double tunnels
		$0.19 < x < 0.33$	HTB
K	0.138	$0.06 < x < 0.10$	ITB; double tunnels
		$0.19 < x < 0.33$	HTB
Ba	0.136	$0.03 < x < 0.05$	ITB; single tunnels
		$0.14 < x < 0.16$	Pentagonal structure
Sn	0.122	$0.04 < x < 0.06$	ITB; single tunnels
		$0.15 < x < 0.18$	ITB; double tunnels
Pb	0.118	$0.03 < x < 0.05$	ITB; single tunnels
		$0.18 < x < 0.35$	TTB[b]
Bi	0.102	$0.02 < x < 0.07$	ITB; single tunnels
Sb	0.080	$0 < x < 0.27$	Perovskite
		$0.12 < x < 0.20$	ITB; double tunnels
In	0.079	$0.20 < x < 0.33$	HTB

[a] Ionic radii are those quoted by Shannon (*10*) and Shannon and Prewitt (*11*) for ions in octahedral coordination.
[b] Tetragonal tungsten bronze structure.

Experimental

M_xWO_3 samples, where M = Sb, Sn, or Pb, were prepared by heating together appropriate amounts of WO_3 and the relevant metal in sealed evacuated silica ampoules. All chemicals were of Specpure grade and supplied by Johnson–Matthey. The Sb_xWO_3 samples were placed vertically in a furnace and reactions carried out at 1233 and 1373 K for 7 days. After heating, the samples were quenched into liquid nitrogen. The Sn_xWO_3 samples were reacted at 1173 K for times of between 12 and 19 days (*8*) and the Pb_xWO_3 samples at 973 or 1073 K for times between 7 and 21 days (*12*). Ba_xWO_3 samples were prepared in a similar fashion but from thoroughly mixed amounts of barium tungstate, tungsten metal, and WO_3, reacted at temperatures within the range 1073–1273 K (*13*).

All samples were examined by X-ray diffraction using a Hägg–Guiner focussing camera employing strictly monochromatic CuK_{α_1} radiation and KCl as an internal standard, taking $a = 0.6292$ nm. Films were measured using a scale exposed onto the film prior to development to compensate for film shrinkage.

High-resolution electron microscope studies of the samples were carried out using a Jeol 200CX transmission electron microscope fitted with a double-tilt goniometer stage and operated with an accelerating voltage of 200 kV. Images were taken at magnifications in the range 500,000–1,000,000×. The objective lens of the microscope had a C_s of 1.2 mm and the objective aperture used to obtain structure images had a radius of 3.5 nm. Electron microscope samples were prepared by crushing a small quantity of bronze crystals in an agate mortar under *n*-butanol. A drop of the resulting suspension was placed on a holey carbon support film and the liquid allowed to evaporate to produce a fine coating of tiny fragments on the grid.

Computed images were calculated on the Joint Cardiff Computing Service's Honeywell 11, DPS-8/70M computer, employing programs FCOEFF and DEFECT (*14*). Multislice calculations were performed using a slice thickness of about 0.38 nm, this being the appropriate length of the unit cell axis of the bronze phases which was aligned parallel to the electron beam. The depth of focus due to chromatic aberration was assumed to be 20 nm. Images were calculated over a range of defocus values and crystal thicknesses.

Results

$Ba_{0.04}WO_3$

High-resolution electron micrographs of $Ba_{0.04}WO_3$ were found to reveal the *ITB* nature of the structure of these bronze phases. An example is shown in Fig. 2. In this figure, the square arrays of black spots represent WO_6 octahedra in a WO_3-like

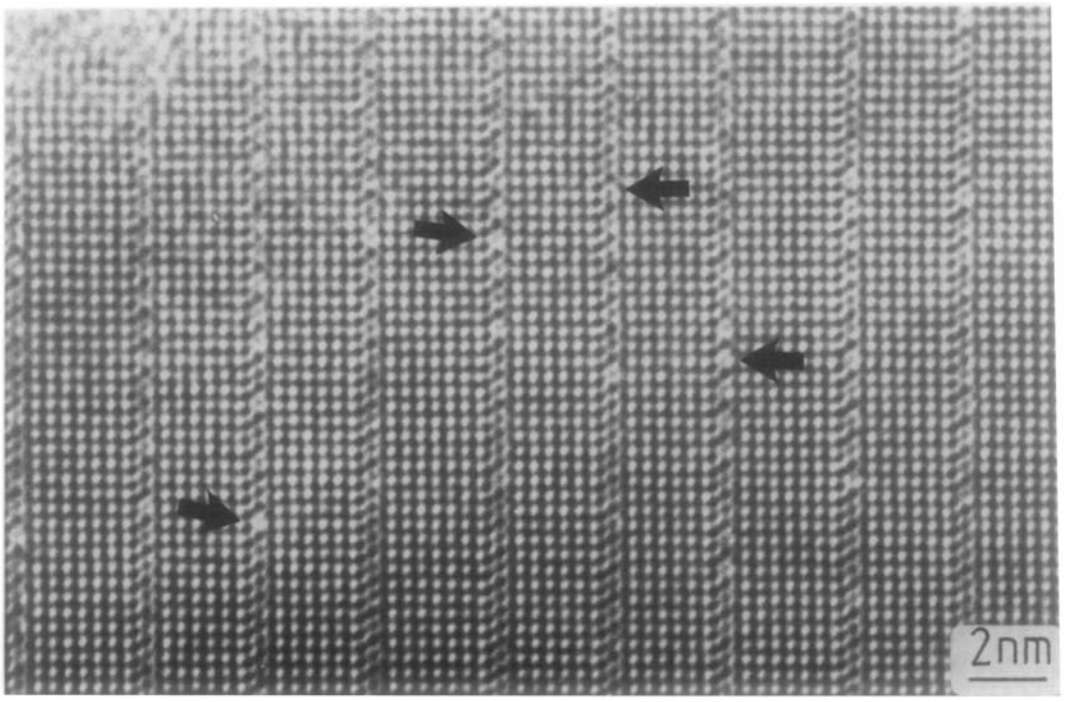

FIG. 2. High-resolution electron micrograph of $Ba_{0.04}WO_3$ viewed down [001]. The cation positions are clearly resolved and reveal that the structure consists of a single row of hexagonal tunnels separated by slabs of WO_3-like material. The occupancy of the hexagonal tunnels is suggested by the variable contrast in these positions, some examples of which are arrowed.

array, and the structure can clearly be seen to be composed of parallel slabs of these WO_3-like regions separated by strips of single hexagonal tunnels. A large number of crystal fragments were examined, all of which showed the same structural type to be present, although a variety of ordered and disordered arrangements of the WO_3-like slabs were observed. The idealized crystal structure of the WO_6 skeleton of a typical member of the series deduced from the images is drawn in Fig. 3.

The barium atoms are presumed to be situated in the hexagonal tunnels. The centers of the tunnel positions show a variable degree of darkening which we believe to be a consequence of the partial filling of the tunnels with Ba. Some tunnels, indicated by arrows in Fig. 2, appear almost completely white and mark the site of empty or

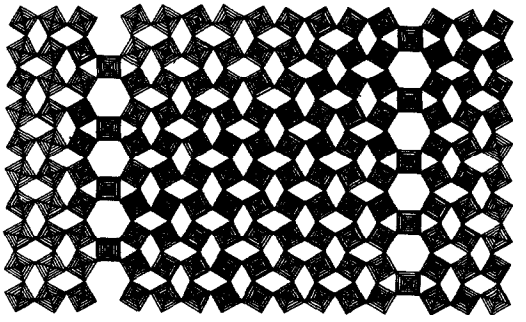

FIG. 3. The structure of one member of the Ba_xWO_3 *ITB* phases viewed down [001]. Only the WO_3 skeleton is shown. The Ba atoms, which have been omitted, are located in the hexagonal tunnels. Other members of the series differ in the separation of the rows of hexagonal tunnels. This structure is also possessed by the Sn and Pb *ITB* phases.

virtually empty tunnels. Computed images are in perfect accord with this model (*15*).

$Pb_{0.04}WO_3$ and $Sn_{0.04}WO_3$

Phase analysis studies on the Pb–W–O system (*12*) showed that a series of bronzes consisting of slabs of WO_3-like structure separated by fault planes existed in the composition range $Pb_{0.03}WO_3$–$Pb_{0.05}WO_3$. A similar set of phases also occurs in the Sn–W–O system (*7, 9*) at similar compositions. Preparation of samples in the composition range $Sn_{0.04}WO_3$–$Pb_{0.04}WO_3$ coupled with powder X-ray phase analysis has shown that a complete solid solution occurs between these phases and that both bronzes appeared to have the same structure. Because of that, we report only the Pb_xWO_3 electron microscope results in detail here.

High-resolution electron micrographs showed that the Pb_xWO_3 crystals were usually very well ordered. Figure 4 is a typical example of the type of fragments found. The fault planes have a complex contrast, as this figure shows. The structure of the fault planes was revealed by high-resolution images obtained over a range of different values of defocus. From these it was found that these Pb-containing bronzes are isostructural with the Ba *ITB* phases. The WO_6 skeleton therefore shows the same form as that illustrated in Fig. 3. The more complex contrast associated with the fault planes is due to the presence of the Pb atoms, which have quite a pronounced effect upon the images recorded. To verify this, computed images were calculated over a wide range of values of defocus using atomic coordinates obtained from idealized structures of the type shown in Fig. 3, in which Pb atoms were placed in all the

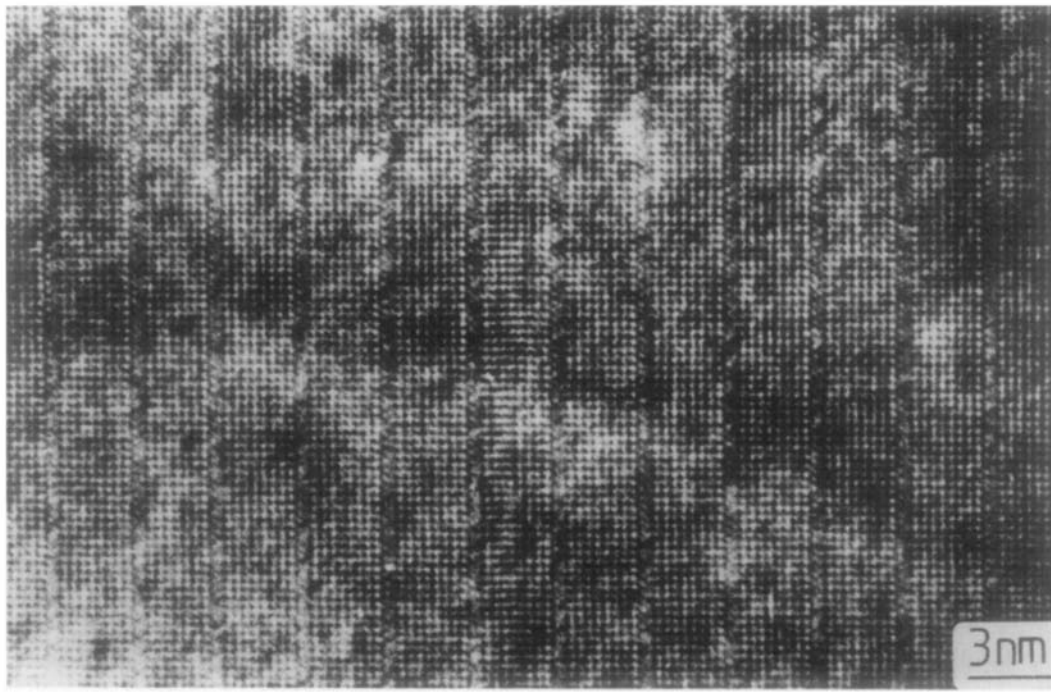

FIG. 4. A high-resolution micrograph of a reasonably well ordered *ITB* crystal from a sample of gross composition $Pb_{0.08}WO_3$.

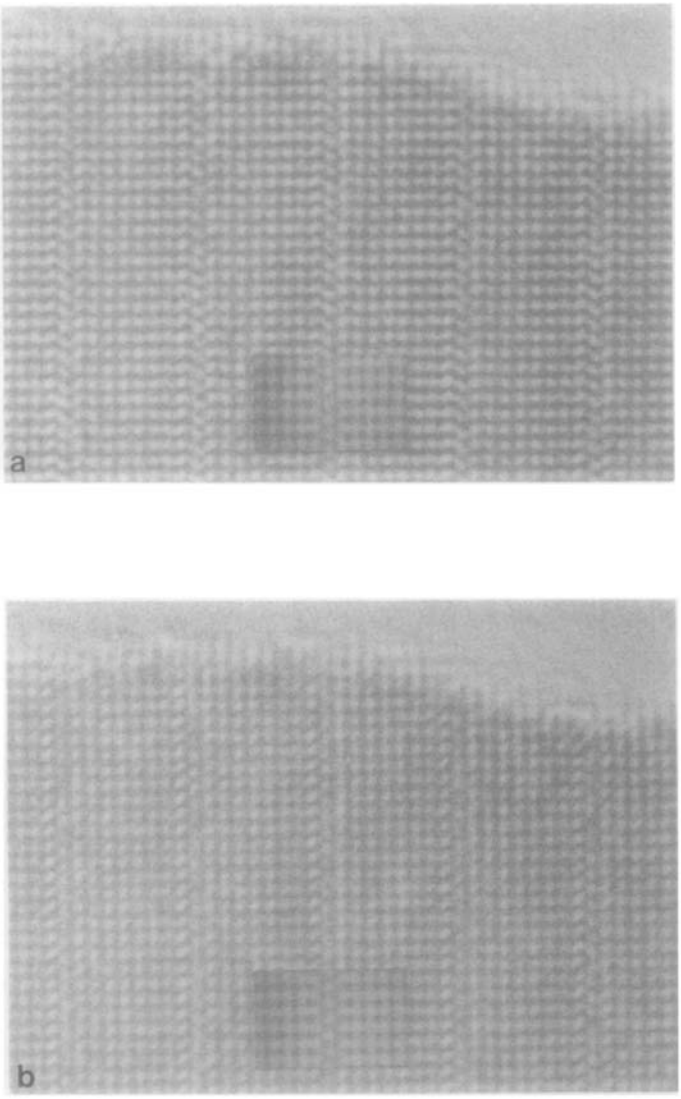

FIG. 5. A sequence of high-resolution micrographs, taken at different defocus values, from a fragment of a Pb *ITB* crystal. In the inset in each micrograph are images computed for defocus values of (a) −4 nm, (b) −10 nm, and (c) −28 nm and 2.9-nm crystal thickness.

tunnel sites. These successfully matched the micrographs obtained, as can be judged from the examples shown in Fig. 5.

Identical studies on the related Sn-containing phases showed that the $Sn_{0.04}WO_3$ bronzes were isostructural with the $Pb_{0.04}WO_3$ phases, confirming the X-ray conclusions.

$Sn_{0.18}WO_3$

Typical high-resolution structure images taken from crystal fragments of bulk composition $Sn_{0.18}WO_3$ are shown in Figs. 6a and b, respectively. The images appear to be quite different from one another. Distinct white blobs of contrast which are

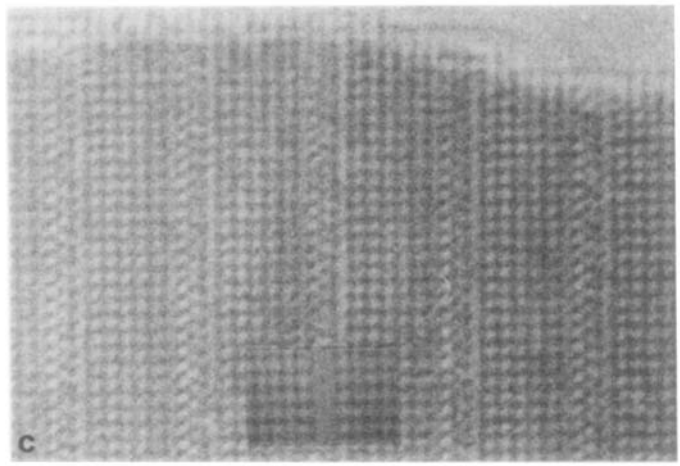

FIG. 5—*Continued.*

visible in Fig. 6a are not present in Fig. 6b. Careful examination of the two micrographs reveals that the contrast in Fig. 6b can be generated from that of Fig. 6a by the insertion of an additional black spot at a position corresponding to the center of each white area. Because the samples were considered to be monophasic, considerable care was taken to ensure that these images were from two consistently found different structure types and not from the same structure viewed in a different projection or under different imaging conditions. The micrographs shown in Fig. 6, typical of those obtained, are from two different through focal series which preserved differences in contrast for all values of defocus which produced reasonable images.

In agreement with this, the diffraction patterns showed that the unit cell sizes for both types of material were the same, within the accuracy of the technique, and corresponded to that of the 5-type structure proposed by Steadman *et al.* (*7*), shown in outline in Fig. 1c. However, the intensities of the reflections on the diffraction patterns of the two materials did differ from one to the other. The contrast in these micrographs is also consistent with the structure shown in Fig. 1c. The high-resolution image shown in Fig. 6a shows a sequence of black dots, the arrangement of which is exactly the same as that shown in Fig. 1c. It is reasonable, therefore, to associate each black spot on the image with a WO_6 octahedron, as above. In Fig. 6b the arrangement is very similar, except that the hexgonal tunnels regarded as empty in Fig. 1c are, in this case, filled. It therefore appears that in our preparations the $Sn_{0.18}WO_3$ phase forms with either filled or empty tunnels. We comment on this further in the Discussion.

Sb_xWO_3

Samples of Sb_xWO_3 in which x took values of 0.15, 0.19, 0.21, and 0.25 all contained dark-blue needle-like crystals which constituted the major component present. X-ray and electron diffraction patterns confirmed that these crystals corresponded to the orthorhombic bronze phase reported by Parmentier *et al.* (*5, 6*). Electron diffraction patterns obtained from the samples of composition $x = 0.25$ invariably produced electron diffraction patterns which were completely ordered, while at compositions closer to $x = 0.15$ variable amounts of streaking occurred in the [100]

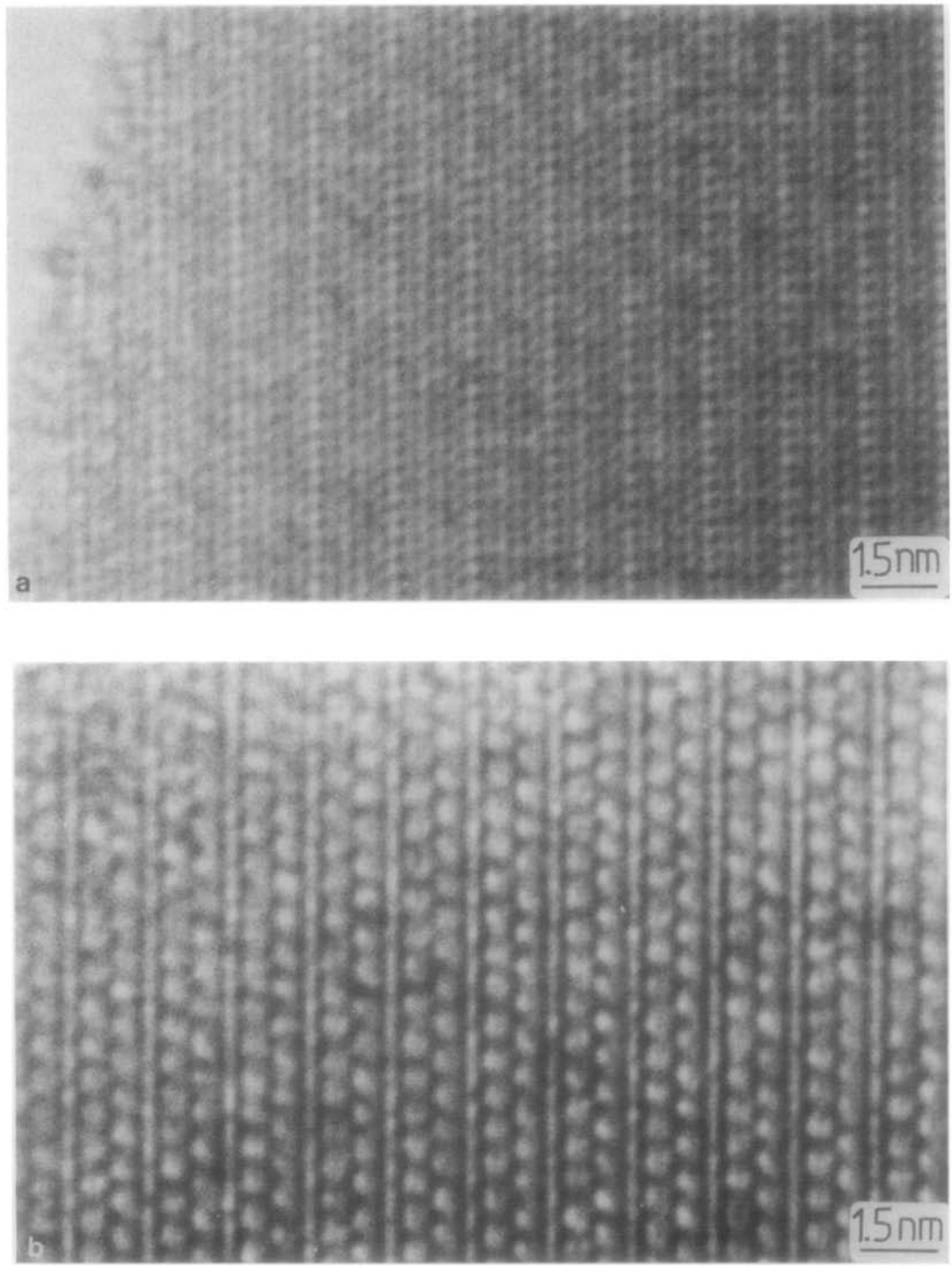

FIG. 6. High-resolution electron micrographs taken from crystal fragments from a sample of overall composition $Sn_{0.18}WO_3$. The images are consistent with materials which have the hexagonal tunnels (a) empty and (b) filled, corresponding to the structure shown in Fig. 1c.

direction, indicative of disorder in the structures. High-resolution electron micrographs mirrored this result; those from the $x = 0.25$ samples showed that the phase was perfect over large regions of crystal while those from lower Sb-containing samples revealed coherently intergrown narrow regions of WO_3-like structure. These two types of microstructure are shown in Fig. 7.

High-resolution micrographs of these samples, as illustrated in Fig. 8, appeared to reveal the presence of hexagonal tunnels, the centers of which were separated by two rows of octahedra. This is in accord with the proposed structure for the ordered phase, the WO_6 octahedral skeleton of which is shown in Fig. 1e. This structure was then used as a model for image calculations, the Sb atoms being introduced into the hexagonal tunnels in accordance with earlier suggestions as to the structure of this phase (*5, 6*). The computed images could be successfully matched to the observed contrast over a range of values of defocus, thus verifying the assumption that the two structures were equivalent. Two examples are shown in Fig. 9. The observed contrast at the thin edge of the crystal in the micrograph of Fig. 9a has been matched to the image computed for −58 nm under focus which is close to the optimum defocus value needed to image heavy atoms as dark contrast. In Fig. 9b the metal atoms are imaged as white spots, which was correlated with a calculated image at a defocus value of −12 nm.

Discussion

The results presented in this paper show that all the phases studied are of the *ITB* type and can be considered to consist of intergrowths between slabs of the *HTB* and WO_3 structures. The Ba, $Sn_{0.04}WO_3$, and Pb bronzes are all characterized by single rows of hexagonal tunnels separated by substantial amounts of WO_3-like structure. The high-Sn-content bronze and the Sb bronze are somewhat different in that the hexagonal tunnels now dominate the structure, the WO_3-like regions being of only one or two octahedra in thickness. These materials are part of an interesting group of nonstoichiometric phases. They only form when the ternary metal is large, an aspect of these phases which has been discussed in two recent publications (*12, 13*) and so here we will concentrate upon the nonstoichiometric nature of these compounds.

The variable composition can initially be considered to be accommodated in two ways, first by varying the atom populations in the hexagonal tunnels and second by varying the ratio of hexagonal tunnels to WO_3-like structure. A variation of filling of the hexagonal tunnels takes place over wide ranges of composition in the *HTB* phases, as is shown in Table I. In view of the structural nature of the compounds, it is germane to inquire whether the same variation in tunnel filling is allowed in the *ITB* phases of interest here. The answer seems to be in the negative for the following reason. The formula of the single-tunnel bronzes, if the tunnels are completely filled by metal M, is given by $M_1(WO_3)_{2n+1}$, where n is the number of WO_6 octahedra separating the M atoms. If we take a typical pair of members of this series, say $n = 8$ and $n = 9$, the compositions are $M_1W_{17}O_{51}$ and $M_1W_{19}O_{57}$, in other words, $M_{0.0588}WO_3$ and $M_{0.0526}WO_3$. Now if the population of the M atoms in the tunnels in the $n = 9$ bronze was able to vary from completely full to just below nine-tenths full, the composition range encompasses the $n = 8$ phase. If any variation of tunnel filling of this order of magnitude was therefore allowed, there would be no need for the formation of a discrete set of phases.

It would seem that this is likely to hold good for all the *ITB* phases discussed here and listed in Table I for the same reason. In

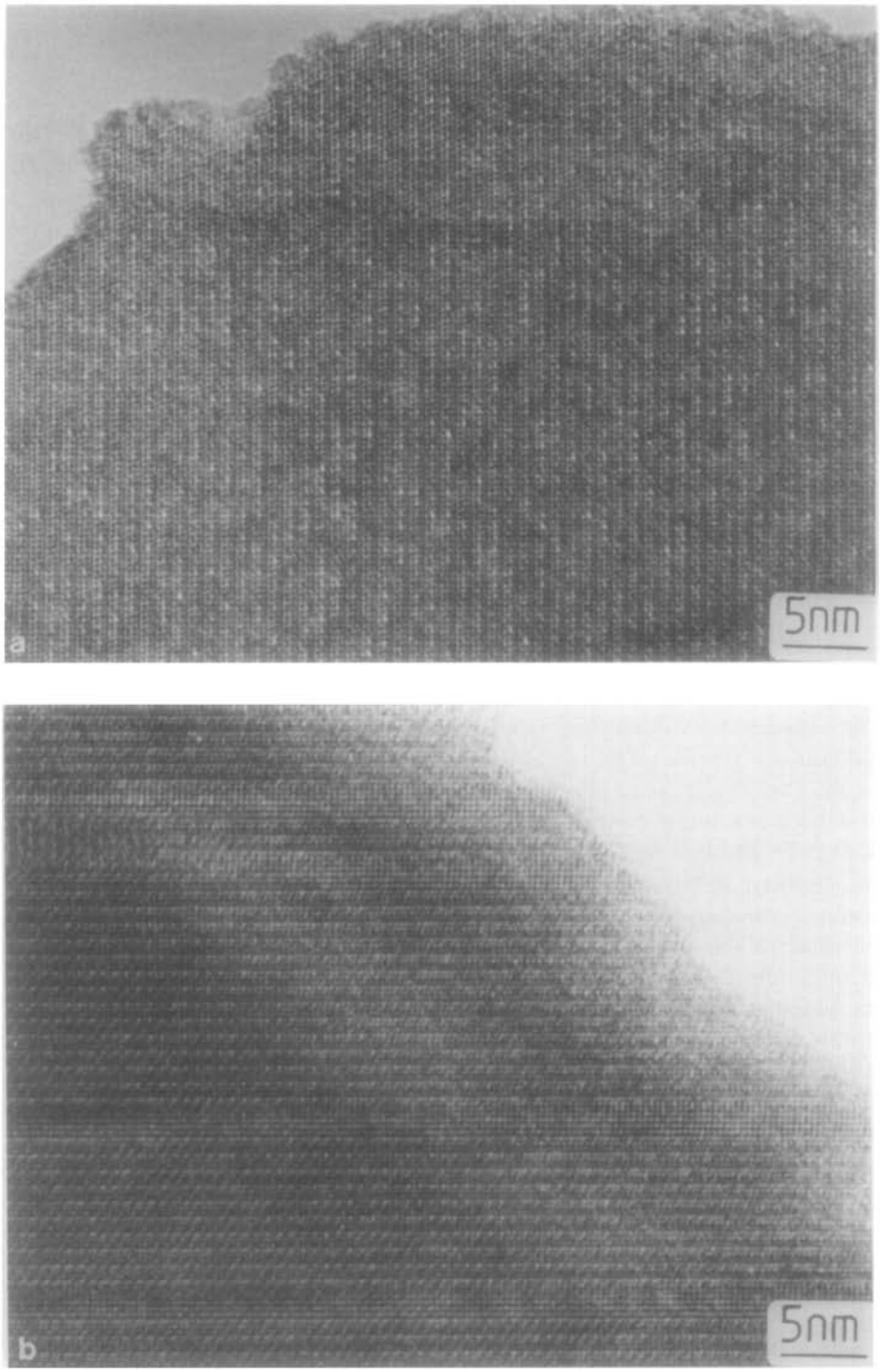

FIG. 7. Electron micrographs of Sb_xWO_3 crystals from samples of overall composition (a) $x = 0.25$ and (b) $x = 0.15$. In (a) the crystals have a perfect structure over large areas. At lower Sb concentrations, narrow regions of WO_3-like structure are intergrown, as shown in (b).

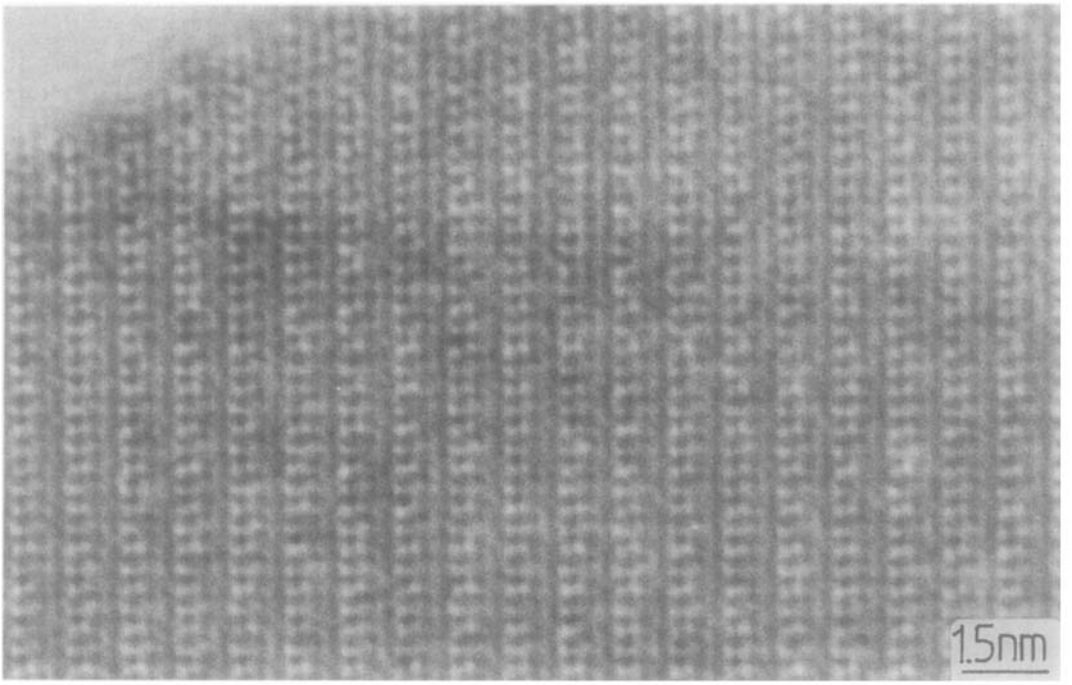

FIG. 8. High-magnification image of $Sb_{0.25}WO_3$. The arrangement of WO_6 octahedra is consistent with the diagram shown in Fig. 1e, with Sb atoms occupying the hexagonal tunnels.

the case of the Sb_xWO_3 bronze, for instance, it is clear that, in our preparations, when the composition fell below $Sb_{0.25}WO_3$, slabs of WO_3 began to intergrow with the bronze. If the tunnels could be filled over the same range of composition as the typical *HTB* phases listed in Table I, then this stratagem would be unnecessary. The same is true of the higher Sn bronzes, which also adopt different structures as the composition changes (*9*).

Despite this, electron micrographs strongly suggest that variable degrees of tunnel occupancy exist. It is possible that this apparent variation, especially in the phases close in composition to WO_3, may be due to artifacts introduced during electron microscope examination. The electron beam has a significant heating effect on the crystals under observation, which may cause the interpolated metal atoms to either evaporate from the thin regions under examination or else to diffuse to other parts of the structure. Such an explanation is less likely in the case of the $Sn_{0.18}WO_3$ samples that were studied, as examination showed that crystals with completely empty tunnels seemed to occur. In these bronzes, it may be that once the template of the structure is laid down in Sn-rich crystals, the skeleton is able to continue growing in the absence of further ternary metal atoms. This is possible in terms of stoichiometry as the skeleton has the composition WO_3. A similar phenomenon has been noted in the related W_5O_{14} phases (*18*).

Turning to the question of the relative amounts of hexagonal tunnel material present, it is clear that this is linked to the amount of ternary metal atom present as just discussed. The exact limits of the existence range of each series, however, cannot be predicted from the results presented here. On the other hand, the results allow

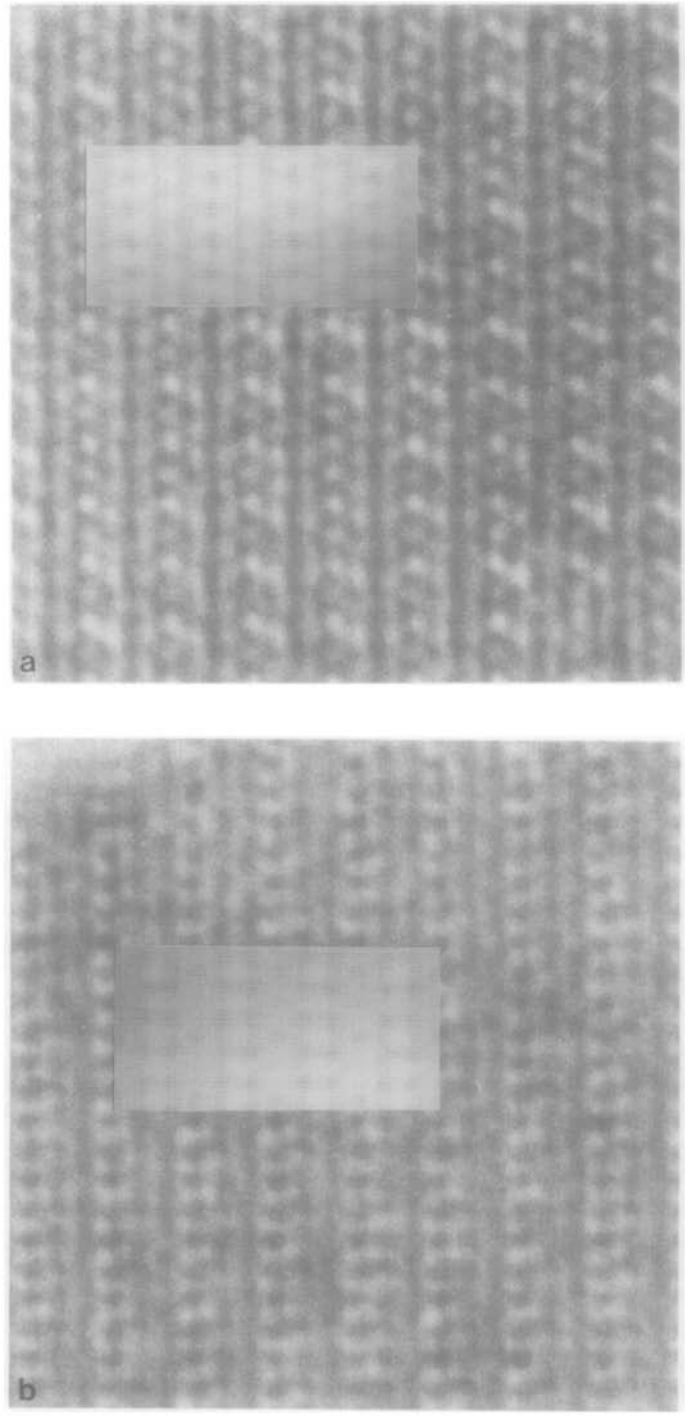

FIG. 9. A comparison of micrographs and calculated images of the Sb *ITB* phase calculated for a crystal 19 nm thick. Defocus values of (a) −16 nm and (b) −58 nm have been matched to the experimental images.

an interesting comparison to be made between the alkali metal *ITB* structures and those found in the Ba, Sn, and Pb systems at low ternary metal concentrations. The alkali metals, together with Tl^+, all form intergrowth bronzes containing double rows of hexagonal tunnels, while the Ba, Sn, and Pb groups form single rows of hexagonal tunnels. These differences are not solely due to differences in concentration of the interpolated ions. In the Ba, Sn, and Pb systems, for example, an increase in the amount of the ternary metals outside of the phase range of the intergrowth bronze does not cause the single rows of tunnels to be replaced by double rows, then triple rows and hence to the complete *HTB* structure. Instead, on the ternary metal-rich side of the phase range, completely new types of structure form. In the case of the alkali metal bronzes, if more alkali metal is present than is required to form the highest member of the double tunnel series, a new structure type forms as a second phase. As before, gradual increase in the number of rows of tunnels eventually leading up to a complete *HTB* structure is not found.

The occurrence of either single or double tunnels is strongly suggestive of valence effects. The alkali metals form M_2WO_4 (i.e., $M_2O \cdot WO_3$) tungstates while Ba, Sn, and Pb all form MWO_4 (i.e., $MO \cdot WO_3$) tungstates in which these metals are divalent (*16*). Thus if the bronzes consisted of WO_3 intergrown with the appropriate tungstate we would expect exactly the same double- or single-tunnel arrangement to occur in order to accommodate the large cations. As the tungstates are fully oxidized, this state of affairs does not hold. However, it is possible that the same valence rules that are obeyed in the formation of the tungstates hold during the formation of the bronzes.

There are a number of ways in which this could operate at a mechanistic level. If the ternary metal is delivered to the growing crystal via a tungstate type of molecule transported through the gas phase, valence requirements would persist and molecules of M_2WO_4 or MWO_4 would arrive which might lead to the development of the structures found. Alternatively, at the growing interface of an intergrowth crystal, local electrical neutrality may have to be preserved. In this case, if each hexagonal site in a surface layer of hexagonal tunnels is filled with a divalent ion, the surface remains neutral. It is impossible to do this with monovalent ions unless a double-tunnel structure is built up.

This idea suggests an explanation for the failure to find intergrowth bronzes of the sort analogous to $Ba_{0.04}WO_3$ in the In_xWO_3 and Sb_xWO_3 systems (*17, 5*), even though In forms a *HTB* structure and Sb forms a tunnel structure closely related to the *HTB* type. In terms of the suggestion made above, it is impossible to both fill hexagonal tunnels at a growing interface completely and also maintain local charge neutrality, as in the case of the single- and double-tunnel bronzes. Thus the structures may be destabilized.

While these ideas are attractive, the cases of Bi, which seems to form single-tunnel bronzes, and Cs, which forms single- and double-tunnel bronzes, are anomalous and need further investigation. To clarify this it will be necessary to compile phase existence data not only for these two bronzes but for all of the *ITB* bronzes for a variety of temperatures, as the structures observed may well be temperature sensitive.

Acknowledgment

M.M.D. and K.A.W. are indebted to I.C.I. plc. for financial support.

References

1. A. HUSSAIN AND L. KIHLBORG, *Acta Crystallogr., Sect. A* **32,** 551 (1976).

2. A. HUSSAIN, *Chem. Scr.* **11,** 224 (1977).
3. L. KIHLBORG, *Chem. Scr.* **14,** 187 (1978–1979).
4. A. RAMANAN, J. GOPAKAKRISHNAN, M. K. UPPAL, D. A. JEFFERSON, AND C. N. R. RAO, *Proc. R. Soc. London, Ser. A* **395,** 127 (1984).
5. M. PARMENTIER, C. GLEITZER, AND A. COURTOIS, *Mater. Res. Bull.* **10,** 341 (1975).
6. T. EKSTRÖM, M. PARMENTIER, AND R. J. D. TILLEY, *J. Solid State Chem.* **34,** 397 (1980).
7. R. STEADMAN, R. J. D. TILLEY, AND I. J. MCCOLM, *J. Solid State Chem.* **4,** 199 (1972).
8. R. STEADMAN, *J. Chem. Soc., Dalton Trans.,* 1271 (1972).
9. T. EKSTRÖM, M. PARMENTIER, AND R. J. D. TILLEY, *J. Solid State Chem.* **37,** 24 (1981).
10. R. D. SHANNON, *Acta Crystallogr., Sect. A* **32,** 751 (1976).
11. R. D. SHANNON AND C. T. PREWITT, *Acta Crystallogr., Sect. B* **25,** 925 (1969).
12. T. EKSTRÖM AND R. J. D. TILLEY, *J. Solid State Chem.* **24,** 209 (1978).
13. T. EKSTRÖM AND R. J. D. TILLEY, *J. Solid State Chem.* **28,** 259 (1979).
14. A. J. SKARNULIS, Ph.D. thesis, Arizona State University, Tempe, 1976.
15. J. L. HUTCHISON, G. R. ANSTIS, AND R. J. D. TILLEY, *in* "Proceedings, 10th International Congress on Electron Microscopy, Hamburg, 1982," p. 57.
16. T. EKSTRÖM AND R. J. D. TILLEY, *Chem. Scr.* **16,** 1 (1980).
17. T. EKSTRÖM, M. PARMENTIER, K. A. WATTS, AND R. J. D. TILLEY, *J. Solid State Chem.* **54,** 365 (1984).
18. T. EKSTRÖM AND R. J. D. TILLEY, *J. Solid State Chem.* **19,** 125 (1976).